Cite this article as:
F. Grisafi, A. Brucato, G. Caputo, S. Lima and F. Scargiali, 2023, Modelling Particle Dissolution in Stirred Vessels, *Chemical Engineering Research and Design*, 195, 662-672.
https://doi.org/10.1016/j.cherd.2023.06.026

Modelling Particle Dissolution in Stirred Vessels

*F. Grisafi, A. Brucato, G. Caputo, S. Lima and F. Scargiali**

Dipartimento di Ingegneria, Università degli Studi di Palermo,
Viale delle Scienze Ed.6 - 90128 Palermo, Italy

ABSTRACT

Particle dissolution in stirred vessels is a unit operation commonly encountered in several production sectors, such as the mineral, pharma and chemical industries. It is commonly conducted batch-wise under time-dependent conditions, a circumstance that complicates model set-up.

This paper presents a set of models for simulating batch dissolution of polydisperse particles in stirred vessels. Models described encompass all cases of particle batch dissolution in stirred vessels, whether the amount of initially added particles is larger or smaller than that needed to achieve solution saturation (hence whether particles are eventually completely dissolved or not) and whether single- or multi-sized particles are dealt with. Convenient model simplifications are also provided for the cases of final solute concentration much smaller than saturation (low final concentration models).

All models are successfully experimentally validated. The single-size large final concentration model is employed to set up experimental runs that, apart from their use in predictive simulations, may be employed for simultaneously measuring mass transfer coefficient and interfacial solute concentration using suitable experimental runs. The ability to measure interfacial solute concentration is also exploited for assessing whether it coincides, or not, with the solute saturation concentration, a common assumption when dealing with solid-liquid mass transfer, which in the present case is found to hold true. The simpler single-size low-final-concentration model is very convenient for measuring the mass transfer coefficient alone. Finally, the multi-size model is utilised to evaluate the sensitivity of the estimated mass transfer coefficient in the single-size model to the particle size range employed during experimental measurements of mass transfer coefficients.

Keywords:

Mixing, solid-liquid agitation, mass transfer coefficient, interface concentration, particle dissolution modelling

Corresponding author

Francesca Scargiali

Università degli Studi di Palermo

Dipartimento di Ingegneria

Viale delle Scienze, 6

90128 Palermo, ITALY

Tel: +3909123863714

email: francesca.scargiali@unipa.it

1. Introduction

Particle dissolution in stirred vessels is a unit operation commonly encountered in several production sectors, such as mineral, pharma and chemical industries. Therefore, suitable models for particle dissolution processes are needed for developing and designing the apparatuses involved. Additionally, these models can be used to measure the solid-liquid mass transfer coefficient, which is important not only in process applications like solid-catalyzed liquid reactions (Grisafi et al.,1998; Pangarkar, 2002), but also in scientific fields such as bio-medical applications and earth sciences, as well as technological applications like well-drilling (Meneses et al., 2017).
It is not surprising, therefore that the topic has attracted significant attention over the years, to develop suitable dissolution models and/or investigating mass transfer coefficient values (e.g. Hixon and Crowell, 1931; Barker and Treybal, 1960; Nienow, 1975; Nienow and Miles, 1978; Kulov *et al.*, 1983; Brucato *et al.*, 1990; Pangarkar *et al.*,2002; Winterbottom *et al.*, 2003; Bayens *et al.*, 2012).

Particle dissolution is commonly conducted batch-wise, hence under time-dependent conditions, a circumstance that complicates model set-up, due to the relevant time variations of particle features and mass transfer driving force. Other modelling difficulties arise from the fact that particles may exhibit size/shape distributions and that diversified outcomes can be expected depending on whether the initial particle mass is larger or smaller than the amount needed for reaching solid-liquid equilibrium. Also, space-dependent features such as solute bulk concentrations, local velocities, particle-liquid slip-velocities and turbulence levels (hence local k_c values), all affect the local particle dissolution rate. The overall mass transfer observed clearly results from the ensemble-averaged history of dissolution rates experienced by each particle while travelling inside the vessel. These last complexities can only be tackled by resorting to complex CFD-based two-phase simulations, as done by Hormann *et al.* (2011), who employed RANS for the liquid phase and Lagrangian DPM for the particles, as well as by Hartman *et al.* (2006), who resorted to LES and an Eulerian-Lagrangian approach involving particle size distribution as well as particle-particle and particle-walls interactions, so usefully getting extremely detailed information, but clearly at the cost of an extremely high simulation burden and suffering from a substantial lack of experimental evidence for model details validation. As concerns this last aspect, advanced experimental techniques such as Electrical Resistance Tomography (ERT, Carletti *et al.*, 2018; Montante *et al.*, 2019) and Laser Sheet Image Analysis (LSIA, Tamburini *et al.*, 2013; Busciglio *et al.*, 2010) have started being employed for getting local features of the stirred two-phase mixtures, including the case of dissolving particles, and may provide the experimental information needed to validate complex CFD models. Apart from these last developments, most of

the previously quoted dissolution models adopt a *concentrated parameter* approach for the interfacial and bulk concentrations as well as for mass transfer coefficient and particle size (*i.e.* time-dependent uniform values for the quoted parameters), and have the advantage of requiring a much simpler mathematical treatment (in most cases resulting in simple algebraic integral solutions) though at the cost of greater or smaller inaccuracies and restrictions of the application field, as discussed in the followings for the assumptions here adopted.

It is worth noting that in most cases, including the advanced CFD models, solute interfacial concentration is typically assumed to coincide with the equilibrium solute concentration, neglecting interfacial resistances. This may well be the case in many instances, but may not be true in other instances, as in the case of particle crystallization, the reverse process with respect to particle dissolution. In any case, the viability of this assumption should be suitably investigated to assess its applicability range. Apart from that, particle equilibrium concentration might be unknown and/or not experimentally measurable, as it occurs for solids giving rise to "incongruent dissolution", a condition in which a different solid phase starts precipitating before reaching equilibrium with the dissolving solute, so inhibiting a meaningful equilibrium to be reached and measured. In such cases expressing the driving force for mass transfer is impossible, even if one is prepared to neglect interfacial resistances. Also, this case clearly underlines the importance of setting up experimental techniques able to measure the interfacial concentration during the dissolution, a topic addressed in the past by one of the present authors (Brucato *et al.*, 1990) and is further explored in this study with improvements.

2. Dissolution models for single-sized solute particles

In the following, the solute flux $\boldsymbol{J}$ at the solid-liquid interface during particle dissolution is assumed to be described by Equation (1):

$$\mathbf{J} = k_c (C_i - C) \tag{1}$$

where the solute flux leaving the solid interface $\boldsymbol{J}$ is given by the product of the mass transfer coefficient k_c and the driving force (C_i-C), with C_i and C being respectively the volumetric concentration at the particle-liquid interface and that in the bulk of the solution. Equation (1) is a definition of the mass transfer coefficient k_c. Its value is independent of solute concentrations, if the simple proportionality between driving force and mass transfer flux postulated by Equation (1) holds true, which is, fortunately, the case for many practical solid-liquid systems.

The other assumptions common to all model developments in the following are:

a) batch system;
b) the liquid phase is perfectly mixed at any time (i.e. solute bulk concentration at some distance from the interface is the same for all particles); this clearly implies that particle dissolution is assumed to be slow with respect to liquid mixing rate (*viz* particle dissolution time significantly larger than mixing time);
c) all particles are suspended (N>Njs) and therefore fully able to participate in the mass-transfer processes;
d) solute dissolution does not significantly affect the volume of the solution;
e) particle shape does not change during the dissolution.
f) particle-solute mass-transfer coefficient k_c is the same for all particles, irrespective of their size, and remains constant during the dissolution;
g) interfacial concentration C_i is the same for all particles and remains constant during the dissolution;

As regards the above assumptions, one may note that:
a) industrial dissolution processes are actually conducted batch-wise in most cases; should this not be the case, the model has to be suitably adapted. The information presented in this paper may still be of help, especially if a continuous dissolution in a plug flow dissolver is performed, as in such case each suspension parcel may be regarded as evolving along the tube length exactly as it would have evolved in time;
b) the liquid perfect mixing hypothesis may not be fully satisfied, especially when dealing with highly soluble particles (small dissolution times) and/or large-scale systems (large mixing times). When this condition is not satisfied the need arises for more complex dissolution models, able to account for spatial variations of both liquid and particle concentrations. An interesting possibility is that of using CFD-based modelling approaches, as quoted in the introduction, but clearly results accuracy has to be so important that the much larger modelling burden is justified. In any case, simple concentrated parameter models, such as the ones described here, can provide quick useful indications, despite quantitative inaccuracies expectable when model hypotheses are not fully satisfied. In any case, for all the data presented hereafter the perfect mixing hypothesis was always very well satisfied being the estimated mixing times smaller by more than an order of magnitude of the concentration dynamics time constant.
c) this simplification is clearly needed because if some of the particles are laid on the bottom as fillets, their contribution to mass transfer would be small and difficult to predict. They would be gradually suspended eventually but in an almost unpredictable way. Moreover, their complete

dissolution would take a much longer time, which is the reason why often dissolution processes are run under full suspension conditions.

d) this simplification is normally acceptable as in most cases volume effects upon dissolution are small enough to be practically negligible.

e) this is a commonly accepted assumption for dissolution, as well as for crystallization, processes. It may not be fully satisfied sometimes, but modelling shape variations would be such a hard job that accepting the assumption and the relevant (small) model inaccuracies is the normal choice.

f) this is also a commonly adopted hypothesis when modelling particle dissolution; it is consistent with the Komogorof theory of turbulence and has received significant experimental verifications (e.g. Brucato *et al.*, 1990, Grisafi *et al.* 1998). It is true that in some cases experimental mass transfer coefficients are found to vary slightly with particle size, also in the hundreds of microns size range of interest for many applications (e.g., Nikade & Pangarkar, 2007). However, it is worth noting that, due to the cube law that relates particle mass to particle size (see Equation 3), when particle size has become only one-half its initial value, almost 90 % of the solute concentration change in the liquid process has already taken place, and therefore results are mainly affected by the average k_c value in a reasonably small size range. Hence, assuming a mean constant value should not entail a significant departure of the model from reality.

g) as concerns this last assumption, the uniformity of Ci for all particles at any given time directly descends from assumption f) while its independence of time deserves some consideration. As a matter of fact, while the dissolution process takes place the mass transfer flux J decreases due to a decrease of the driving force (C_i-C) while C increases. In case there were significant interfacial resistances, these would make C_i smaller than the equilibrium concentration C_{eq} by a larger amount the larger the flux $\boldsymbol{J}$, so leading to larger values of Ci (values closer to C_{eq}) while time elapses. The present assumption is therefore exactly verified only if interfacial resistances are negligible throughout the dissolution process, in which case the interfacial concentration always practically coincides with the equilibrium concentration C_{eq}.

2.1 Single-sized solute particles and large final solute concentrations

If all particles added to the liquid phase at the start of the batch do share the same particle size, because of the a) and b) hypothesis above, their size will decrease at the same rate for all of them, so resulting in a uniform particle size at any instant, yet a smaller and smaller size as time elapses.

By coupling Equation (1) with the mass balance on the dissolved solute, under the above hypothesis, the following equation is obtained:

$$V_t dC/dt \;=\; k_c S_t (C_i - C) \qquad (2)$$

where S_t is the total particle surface area exposed to the liquid.

During the dissolution, particle size decreases leading to a decrease in particle-liquid interfacial area. Remembering that particle shape is assumed not to change during the dissolution process, the volume and the interfacial surface of one particle can be expressed by the following equations:

$$V_p = \alpha\, d_p^3 \qquad ; \qquad S_p = \beta\, d_p^2 \qquad (3)$$

where d_p is a suitable particle characteristic size and α and β are the volume and area shape factors respectively. By denoting with C_0 the concentration in the liquid phase at time zero, with M_0 the mass of solids added to the liquid at the same time and with C and M the solution concentration and the mass of undissolved solid particles at time t, respectively, the overall mass balance on the solid particles ($M_0 + VC_0 = M+VC$) may be rewritten as:

$$d_p = d_{p0}\,(\,1 - x\,)^{1/3} \qquad (4)$$

where d_{po} is the starting diameter of the particles and x is the dimensionless concentration in the liquid phase defined as:

$$x \;=\; \frac{C - C_0}{C^* - C_0} \qquad (5)$$

where C^* is the concentration that the liquid phase would attain in the hypothesis of complete dissolution of the solid phase ($C^* = C_0 + M_0/V_t$). Please note that C* only depends on the initial solute concentration and the added solute mass at time zero (M_0). As such, C^* may well be greater than the solute saturation concentration, in which case, particles will only be partially dissolved when the solution bulk concentration approaches the interfacial concentration and mass transfer ends.

The total particle surface exposed to the liquid at any time during the dissolution process can be written as:

$$S_t \;=\; \frac{(\beta/\alpha)\, M_o}{\rho_p\, d_{po}}\,(\,1 - x\,)^{2/3} \qquad (6)$$

Substituting Equations (5) and (6) into Equation (2), leads to:

$$\frac{dx}{dt} = A\,(1 - x)^{2/3}\,(x_i - x) \tag{7}$$

Where the interfacial dimensionless concentration x_i is given by:

$$x_i = \frac{C_i - C_o}{C^* - C_o} \quad ; \quad A = k_c\,(\beta/\alpha)\,\frac{C^* - C_o}{\rho_p\, d_{po}} \tag{8}$$

and where A is a multiplying factor simply proportional to k_c, with dimensions of time^{-1} (*e.g.* s^{-1}) as can be inferred by the dimensionless nature of all items but t in Equation 7

Equation 7 shows that the slope of the time dynamics of x *(i.e. C)* will flatten, tending to the relevant horizontal asymptote, when x approaches either the value 1 or x_i, and precisely to the smallest of the two, as this is the one that will be encountered first while concentration increases. This confirms the ability of the present model to deal with both the cases:

i) when the mass of particles initially added to the system is insufficient to saturate the solution ($C_i > C^*$, $x_i > 1$), in which case all particles are eventually dissolved and the final concentration value is C^* (x=1);

or

ii) when the mass of particles initially added to the system is more than sufficient to saturate the solution ($C_i < C^*$, $x_i < 1$), in which case all particles are eventually dissolved and the final concentration value is C_i or $x = x_i$.

Luckily enough, with the initial condition $x = 0$ at time $t = 0$, an analytical solution of Equation (7) exists, and can be written as:

$$\frac{1}{y_i^2}\left\{\frac{1}{2} ln\left[\left(\frac{1-y_i}{y-y_i}\right)^3\left(\frac{y^3-y_i^3}{1-y_i^3}\right)\right] + \sqrt{3}\,arctan\left(\frac{2y+y_i}{\sqrt{3}y_i}\right) - \sqrt{3}\,arctan\left(\frac{2+y_i}{\sqrt{3}y_i}\right)\right\} = A\,t \tag{9}$$

where:

$$y = (1-x)^{1/3} = d_p/d_{p0} \quad ; \quad y_i = (1-x_i)^{1/3} \tag{10}$$

which is similar to the *Cube Root Law* introduced by Hixson and Crowell (1931). It may be worth noting that Equation (9) is explicit for t while it cannot be made explicit for y. Therefore, when using it, it is better to provide a value for y and use Equation 9 to obtain the time at which the given y value is achieved.

In practice equation 9 provides a two parameter algebraic equation that can be employed either for predicting systems behavior when the two parameters A and y_i are known, or for assessing

their values by best-fitting model predictions to purposely obtained experimental data. From the A and y_i values so obtained, values for both mass transfer coefficient k_c and interfacial concentration C_i respectively, are immediately obtained.

Clearly Equation (9) can deal with all cases of batch dissolution, whether the solid mass initially introduced is bound to be completely dissolved ($x_i>1, y_i<0$), or not ($x_i<1, y_i>0$). In practice, y (i.e. d_p/dp_0) is 1 for t=0 and gradually decreases while time elapses and particle size reduces, up to asymptotically approaching y_i. In case $y_i > 0$ (added particle mass able to saturate the solution) the final (asymptotic) value of d_p will be given by $y_i\, d_{po}$. On the contrary, if $y_i < 0$, the y values maintain their physical meaning only as long as they are larger than zero (as a negative particle size has no meaning) and the intersection of the y curve with the t axis marks the time at which particles vanish from the system, i.e. *particle dissolution time* t_{diss}:

$$t_{diss} = \frac{1}{Ay_i^2}\left\{\frac{1}{2} ln\left[\left(\frac{y_i-1}{yi}\right)^3\left(\frac{y_i^3}{y_i^3-1}\right)\right] + \sqrt{3}\, arctan\left(\frac{1}{\sqrt{3}}\right) - \sqrt{3}\, arctan\left(\frac{2+y_i}{\sqrt{3}y_i}\right)\right\} \qquad (11)$$

Equation (11) resembles that developed by Baeyens et al. (2012) and might be employed for assessing k_c values on the basis of experimental dissolution times, as actually done by the same authors. It is worth noting that such techniques are subject to uncertainties in the assessment of dissolution times, due to subjectivity and to the circumstance that particle systems almost always show a larger or smaller size distribution, hence the dissolution time observed is likely to be close to that of the largest particle in the system, while the bulk solute concentration dynamics rather depends on all particles introduced. It is for this reason that, in the authors opinion, k_c measuring techniques based on experimental solute concentration dynamics, which depends on all dissolving particles, as done for instance, by means of a differential model, by Meneses *et al.*, (2017), should be preferred to techniques based on dissolution time observation.

Finally, in the particular case of $y_i=0$ (i.e. $C^*=C_i$; $x_i=1$) Equation (9) leads to indeterminate results; in this case, however, integration of Equation (7) is straightforward as the two rightmost factors in the R.H.S. of Equation (7) can be combined into one, and the solution of Equation 7 simply becomes:

$$y = \left(\frac{3}{2}At + 1\right)^{-\frac{1}{2}} \qquad (12)$$

2.2 Single-sized particles and low final solute concentration

Equation (7) can be simplified if the mass of particles initially added to the system is much smaller than the mass needed to saturate the liquid. In this case in fact $x << x_i$ during the whole run, and therefore $x_i - x \approx x_i$ the analytical solution of the resulting differential equation is much simpler:

$$y = 1 - \left[k_c(\beta/\alpha) \frac{C_i - C_0}{3\ \rho_p\ d_{p0}} \right] t \qquad (13)$$

which in practice coincides with that employed by Nienow and Miles (1978). Equation (13) can be put in the form:

$$d_p = d_{p0} - B\ t \qquad (14)$$

where:

$$B = A\ d_{p0}\ \frac{x_i}{3} = k_c(\beta/\alpha) \frac{C_i - C_0}{3\ \rho_p} \qquad (15)$$

Plots of t *vs* d_p should then appear as straight lines passing from (t_0, d_{p0}), and with a slope B simply proportional to k_c (Equation 14). This makes this model very convenient for carrying out k_c measurements: all is needed is to run an experiment complying with model hypothesis (single-sized particles, low final concentration, well-mixed liquid phase etc.) and, from the experimentally assessed slope B, a value for k_c is immediately obtained by Equation (15). Clearly in this case the interfacial concentration value cannot be assessed, as a difference from the large final concentration runs.

3. Experimental

Experimental runs were performed to validate the models. These were conducted in batch: a stirred vessel was filled with the desired liquid phase and, at time zero, a known amount of solid particles was added to the batch while monitoring the dissolved solute concentration.

Two different stirred vessels were employed for the experimentation:

a) a cylindrical stainless-steel vessel 0.13 m in diameter, provided with a dished bottom and four standard baffles, stirred by a square pitch propeller ($6.86*10^{-2}$ m diameter), offset from vessel bottom by 1/3 of liquid height;
b) a cylindrical vessel 0.19 m in diameter, flat-bottomed, fully baffled and stirred by a Rushton turbine (D=T/2), placed at 1/3 of the liquid height from the bottom;

The dissolution temperature was always maintained at 25°C.

All runs were performed using accurately sieved salt particles so that a narrow size distribution was attained. Particle size varied from 137 μm to 900 μm. Care was taken in order to ensure that during all runs all the particles were suspended.

As solid phases either NaCl or K_2SO_4 or $K_2Mg(SO_4)_2 \cdot 6(H_2O)$ (Schönite) were used.

Salt concentration in the liquid phase was monitored by means of a conductivity meter whose readings were checked against previously determined calibration curves. The time constant of the conductivity measurement apparatus adopted was experimentally found to be smaller than 2 s.

As concerns the liquid phase, for Sodium chloride and Schönite particles, a solution of 30% water - 70% ethylene-glycol (by weight) was used to suitably slow down the particle dissolution rate. In this way the resulting dissolution time constant was always much larger than both the conductivity-meter time constant and stirred vessel mixing times. The viscosity of the solution was experimentally assessed to be $5.84*10^{-3}$ Pa*s. In the case of potassium sulphate particles distilled water was employed in all experimental runs.

4. Models validation for single-sized particles

4.1 Validation of the model for single-sized-particles and high-final-concentrations

Sodium Chloride particles (d_{p0}=$0.45*10^{-3}$ m) were dissolved in vessel a) in the water-glycol solution stirred at N=1100 rpm. More NaCl than needed to attain the saturation was initially added to the system ($C^* = M_0/V_t$ = 153.7 kg/m^3; C_{sat} = 133.9 kg/m^3). Solute concentration dynamics obtained is shown in Figure 1 as dimensionless concentration x vs t values. The x experimental values (empty circles), as expected, start from zero and gradually increase towards a horizontal asymptote at $x = x_i = 0.871$ ($C = C_{sat}$).

For the same data, assuming that C_i coincides with C_{sat} (i.e. neglecting interphase mass transfer resistances, as it is often made in multiphase mass-transfer) and adjusting the A parameter to the value 1.9 s^{-1}, model predictions were obtained through Equation 9. To this end, for each given x value the corresponding y value was computed by Equation 10, and then Equation 9 was employed to directly compute the time t at which the given x value is achieved. By reporting the (x,t) data so obtained in Figure 1, the solid line representing model results was obtained.

As it can be seen, model results fit remarkably well experimental data, thus suggesting that for the investigated system all model assumptions from a) to g) are sound enough for many, if not all, modelling purposes.

Also, the hypothesis of negligible mass transfer resistances ($C_i = C_{sat}$), is found to be sound, at least for the mass transfer rates here at stake. Notably, this seems to be one of the very few experimental confirmations of the soundness of the last assumption in the scientific literature, due to the obvious difficulties in measuring interfacial concentrations, and the present model might well be employed for exploring the range of validity of this assumption in practical cases.

Finally, from the experimentally assessed slope A the mass transfer coefficient k_c could be immediately derived if a value for β/α were available (*e.g.* for spheres and cubes, $\beta/\alpha=6$, then $k_c=0.0020$ m/s). If not, the product k_c (β/α) at the given conditions is available anyway, and this is in practice all one needs for all design and development simulation needs.

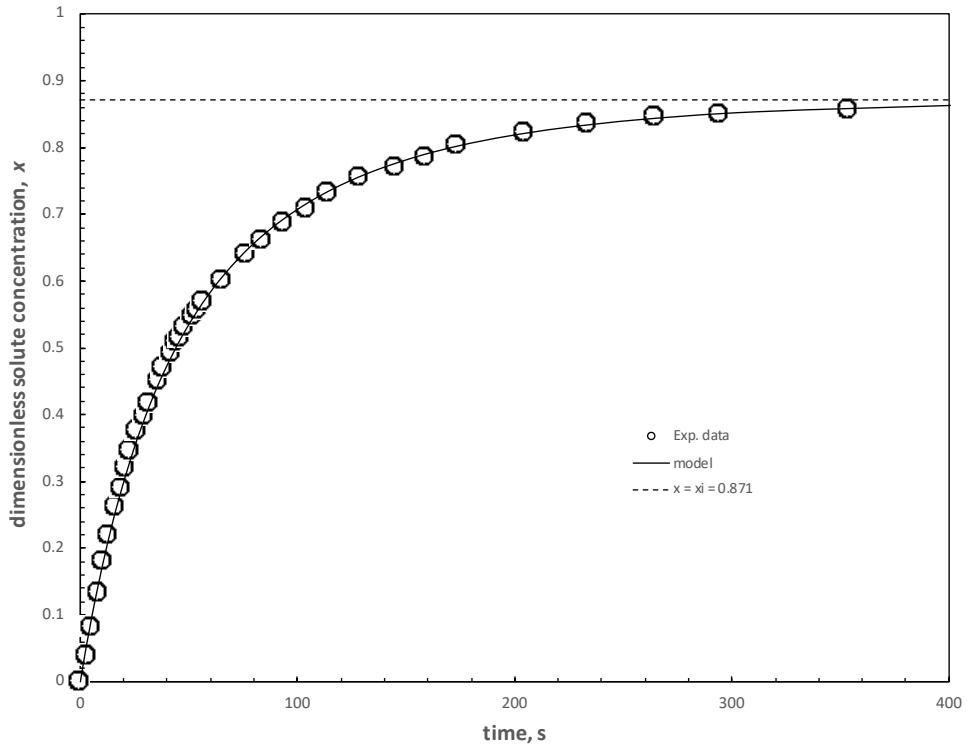

Figure 1: NaCl dissolution (d_{p0}=0.45*10^{-3} m, C_0=0, C*=153.7 kg/m^3, N=1100 rpm): comparison between experimental data (circles) and model predictions for $C_i = C_{sat}$ = 133.9 kg/m^3 (x_i=0.871)

To explore the sensitivity of model results to the interfacial concentration Ci, Equation (9) is rewritten as

$$f(y) = A\ t \qquad (16)$$

As it can be seen, one should expect that if all model assumptions were reasonably abode, plotting the experimental values of *f(y)* versus time should result in a straight line passing from the origin and with a slope equal to A. The function *f(y)* was computed for the same NaCl dissolution data of Figure 1, on the basis of the experimental y values and three x_i values: the first obtained by assuming $C_i = C_{sat}$ = 133.9 kg/m3 (*i.e.* $x_i = 0.871$) and the other two either reduced or increased by 5 % with respect to it. Results are plotted in Figure 2 and, as it can be seen there, the base case $x_i = 0.871$ is the only one practically resulting into the expected straight line, while in both of the other two cases linearity is markedly lost, as testified by the relevant R^2 linear regression values.

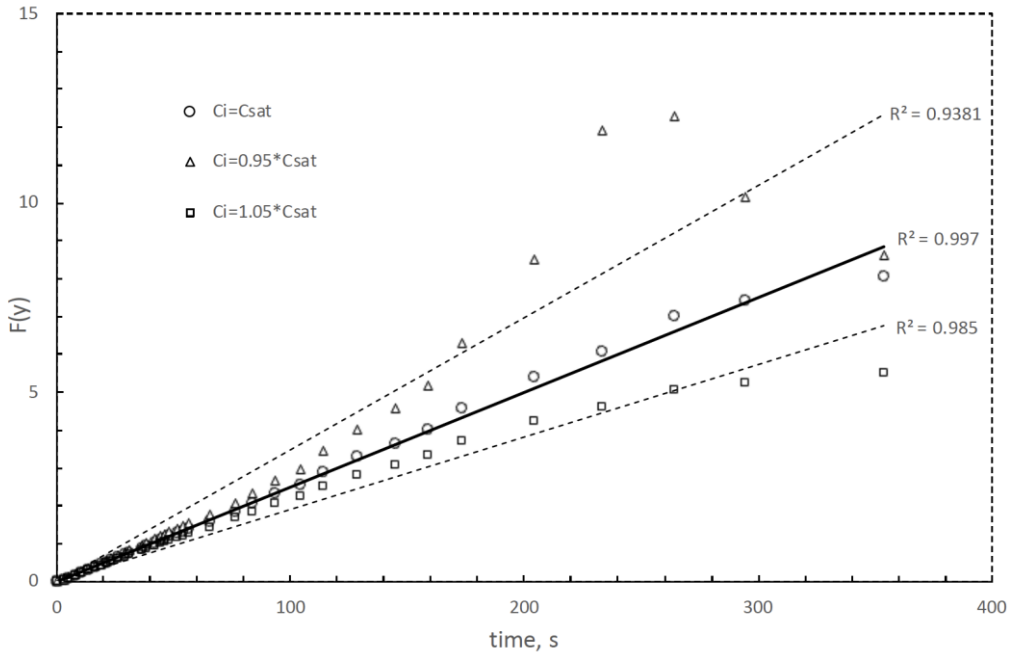

Figure 2: NaCl dissolution, same data as in Figure 1, *f(y) vs t* in relation to three different values of x_i .

Hence, by looking at the effects of the choices for x_i (*i.e.* for C_i), the value that best straightens-up data points can be selected, and from the slope of the straight line a value for *A* (hence k_c) is immediately obtained. In other words, by analysing the data points of a single experimental run, both the value the mass transfer coefficient and the value of the interfacial concentration can be obtained. The same values may then be employed to directly compare experimental concentration dynamics with model predictions, as done in Figure 1, as a check of the suitability of the C_i and k_c values so obtained for interpreting the experimental data. In practice, using the full model and the entire range of data, A and x_i are precisely identified.

4.2 Single-sized high-final-concentrations runs for particles with unknown saturation concentration: the case of Schönite dissolution.

As already pointed out, there are cases in which no reliable solubility data are available, nor can they be experimentally assessed by measuring the concentration attained when the solution is allowed to reach saturation, under the required temperature and pressure conditions.

This is, for instance, the case of the dissolution in water of "Schönite" ($MgSO_4\ K_2SO_4\ 6H_2O$), a salt involved in processes aimed at K_2SO_4 production. As a matter of fact, when Schönite is dissolved into water, the solution gets saturated with respect to Potassium Sulphate before saturation with respect to the former salt is attained. After this point, Schönite dissolution continues (its solubility has not been reached yet) while further precipitation of K_2SO_4 occurs. This property completely inhibits the possibility of experimentally accessing the value of the Schönite saturation concentration, information that, understandably, is unlikely to be found in the literature either.

For this reason, a problem arises in the estimation of the interfacial concentration C_i, even if one assumes that it coincides with the saturation concentration. In such cases, the present model's ability to assess both k_c and C_i by best fitting the predicted concentration dynamics to the purposely obtained experimental data can conveniently be exploited.

In order to assess the interfacial concentration of Schönite during its dissolution, several experimental runs were performed in stirred vessel A, by initially adding a mass of solids that, once completely dissolved, resulted in a final solution concentration of 8.61 kg/m^3, slightly smaller than that at which potassium sulphate precipitation starts (9.0 kg/m^3), as assessed in preliminary runs. A typical result obtained with Schönite particles is shown in Figure 3, where it can be observed that the agreement between experimental data and the predicted dissolution curve (solid line) is very good for the best-fitted parameter values. This finding implies once again that all assumptions involved in the derivation of Equation (9) hold true, within experimental error, also in the case of Schönite particle dissolution.

To show the discriminating power of this technique, in the same Figure other curves relating to different values of the two parameters have been plotted. It can be observed that a +20% change in the value of the mass transfer coefficient (hatched line, A=6.57*10^{-4} s^{-1}) leads to clearly missing all experimental data. Though not shown, a similar increase of the interfacial concentration (x_i) would have led to a similarly neat discrepancy, while reducing x_i by 20% (x_i=1.743) results in the dotted line in Figure 3, which is similar to what would have been obtained by underestimating A by 20%.

One may wonder, however, what happens when at the same time one of the two parameters is underestimated while the other is overestimated. As a matter of fact, an inspection of Equation (7) reveals that at short dissolution times, when x is still close to zero, it is the product of the two

model parameters that determins the predicted concentration dynamics. To assess whether results can be fooled by contextual under- and over-estimations of the two parameters, the dotted line has been computed and added to the experimental data in Figure 3. In this case, A has been overestimated by 20%, with

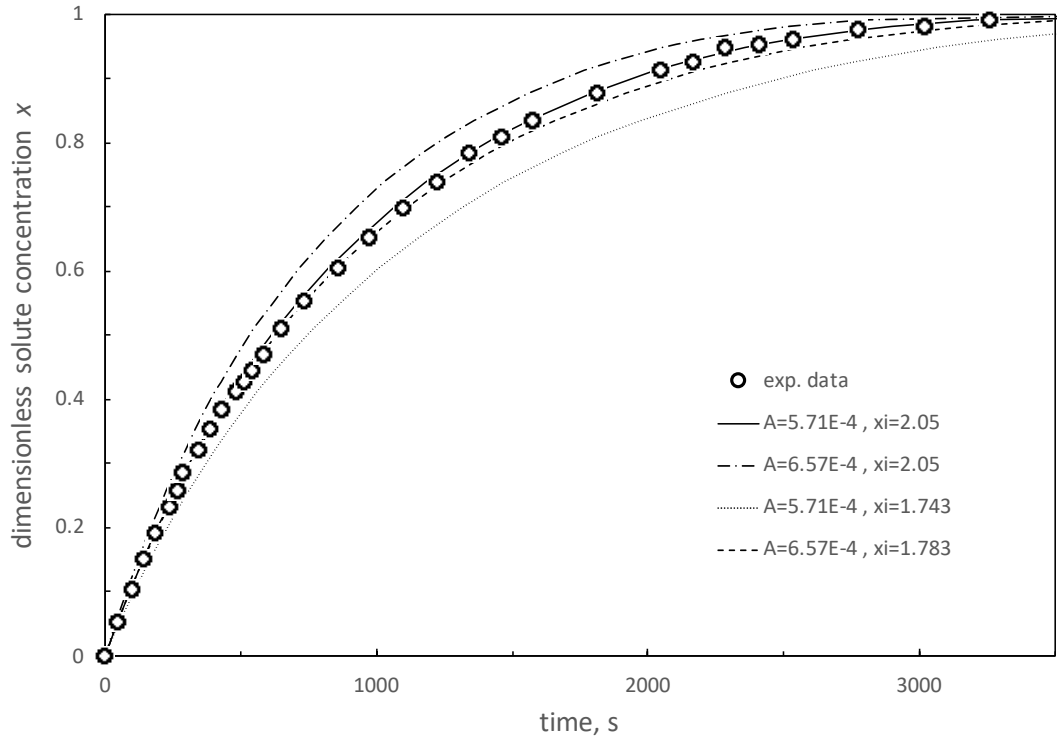

Figure 3: Time dynamics of Schönite dissolution in water-glycol solution: comparison between experimental data (circles) and model predictions (lines). Agitation speed 900 rpm, d_{p0} =0.9*10^{-3} m, C*= 8.61 kg/m^3.

respect to its best-fit value, while the dimensionless interfacial concentration x_i has been underestimated by slightly less than 20% (A=6.57*10-4, xi=1.783) in such a way that the two parameters product is identical to that of the best-fit case. The results are reported as a dashed line, and as it can be seen, this time at short times the predicted concentration dynamics practically coincide with the best-fit case, as expected. At longer times, however, the predicted dynamics detach from the best-fitting case and quite neatly miss the experimental data. It can be concluded that the discriminating power of the technique is quite high, as even deviations by very few per cent can be easily spotted.

Other high-concentration experimental runs, characterised by different values of d_{p0} and/or N, were performed and gave rise to similar results. Moreover, the best-fit value of the interfacial concentration was always the same (C_i = 17.7 kg/m^3), independently of agitation speed, hence

independently of k_c. This finding is consistent with the assumption of negligible interfacial mass transfer resistances and implies that the measured interfacial concentration coincides with the Schönite saturation concentration, which could therefore be considered as being assessed.

4.3 Validation of the model for single-sized-particles and low-final-concentrations

A set of low-concentration runs was also performed to validate the simplified model in the case of low-final-concentration runs. Equations 14 and 15 were used to compute the particle diameter from concentration data and the results are shown in Figure 4 in terms of instantaneous particle diameter *vs* time. It can be observed there that the experimental data (symbols) lie along straight lines, as expected. Some departure from the predicted straight line of the last data points in each run depends on the fact that the functional form of Equation (4) amplifies the experimental reading error for points close to the final asymptotic concentration. From the slopes of these lines, assuming $\beta/\alpha=6$, the two k_c values were computed (Equation 15) as being 1.624*10-4 m/s and 1.514*10-4 m/s for the larger and the smaller particles respectively. The two values are close, but not exactly the same, as it could have been expected due to the quite large size of the particles involved. Interestingly, though with the model employed, k_c is assumed to be independent of d_p and this is not exactly the case here, the measuring technique maintains however a significant viability, especially if the regression analysis is limited to the first portion of the dissolution curves.

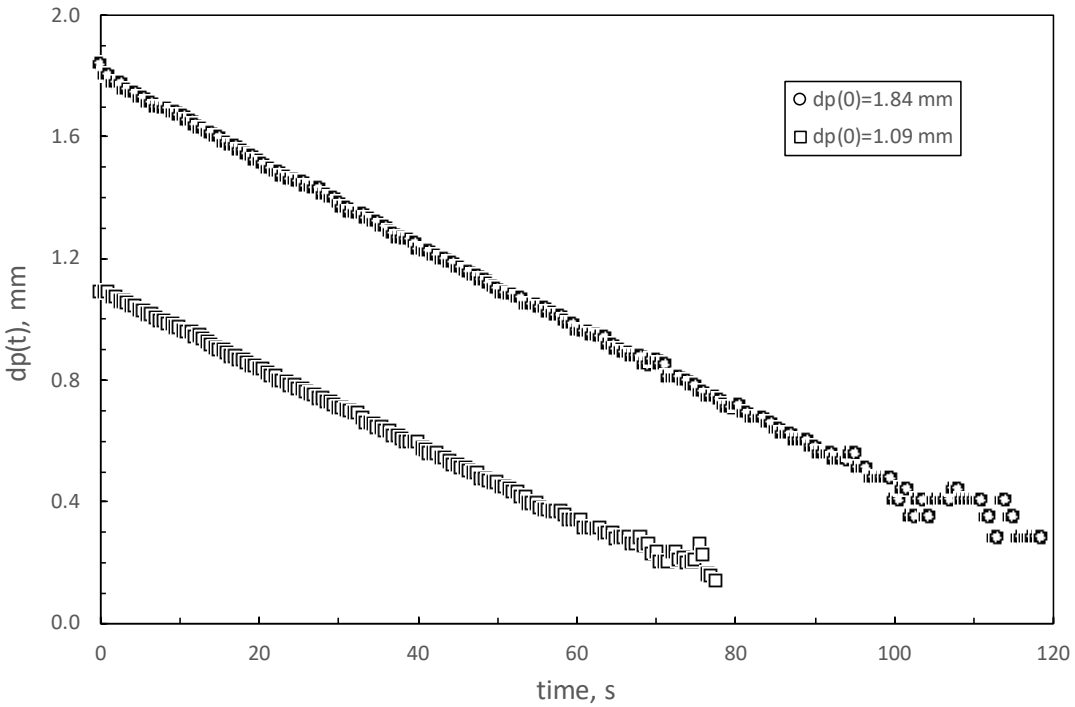

Figure 4: Particle size *vs* time for K_2SO_4 dissolution water (vessel B, N=600 rpm).

5. Particles with size distribution

One of the restrictive assumptions of the models described so far is that all solid particles are assumed to share the same size at the beginning of the dissolution process. This assumption, however, is never perfectly satisfied in real conditions. Removing the restriction of single sized particles is therefore useful to extend the applicability of dissolution models.

Also, when performing experimental runs for mass transfer coefficient investigations, the particles employed for the experimentation are usually sieved and therefore characterized by a particle size range more or less narrow, but certainly much wider than the single size assumed in the dissolution models discussed so far. The problem, therefore, arises of assessing to what extent this neglected feature of real conditions is bound to affect the k_c values obtained. Or conversely, to assess which is the maximum width of the size range that can be afforded while negligibly affecting the k_c measurement.

For the above reasons, the dissolution model was extended to the dissolution of multi-sized particle systems. The extended dissolution model developed is based on the same set of assumptions previously postulated, apart from the hypothesis of single-sized particles, which is replaced by a known initial population density of the particles $n_o(L)$ where L is particle size, adopted here in place of d_p in order to conform to the usual population balance formulations. To properly model particle dissolution in this case, the relevant population balance was written, resulting in the following differential equation:

$$\frac{\partial n}{\partial t} - R\frac{\partial n}{\partial L} = 0 \qquad (17)$$

where n is the (population) number density function at time t, R is the dissolution rate, defined by $R = -dL/dt$, which is assumed to be independent of particle size L, as already done in the case of single-sized particles.

Integration of the above partial differential equation by means of the *characteristics method*, under the initial condition that the population density function n at time zero is $n_o(L)$, leads to the formal solution:

$$n(L,t) = n(L+\Delta L, 0) = n_o(L+\Delta L) \qquad \text{for } L \geq 0 \qquad (18)$$

where:

$$\Delta L = f(t) \;=\; \int_0^t R d\tau \tag{19}$$

Equation (15) implies that, as time goes on, the dissolution process merely results in a progressive shift of the initial distribution function $n_o(L)$ along the length axis (towards the left), the shape of the distribution remaining unchanged. The dissolution rate R may be expressed by writing the mass balance on a single particle:

$$R = \frac{\beta k_c}{3\alpha\rho_p}(C_i - C) \tag{20}$$

Equations (16) and (17), together with mass-balance considerations, lead to the following equation relating the bulk concentration C to particle size shift ΔL:

$$C = C_0 + M_0/V_t - \rho_p \alpha \int_0^\infty L^3 n_o(L + \Delta L) dL \tag{21}$$

Equations 17-21 have been solved, case by case, by means of a simple numerical procedure, leading to the prediction of solute concentration dynamics during dissolution.

It is worth noting that in cases where the amount of solid particles initially added to the system is small in comparison with the quantity that would lead to the saturation (low final concentration runs), it is possible to simplify the governing equations. In this case, in fact, the dissolution rate becomes independent of time:

$$R \cong \frac{\beta k_c C_i}{3\alpha\rho_p} = constant \tag{22}$$

allowing for an easier integration of Equation (21) and leading to the following integral solution:

$$C(t) = C_0 + M_0/V_t - \rho_p \alpha \int_0^\infty L^3 n_o(L + R\ t) dL \tag{23}$$

5.1 Experimental validation of Equation 23

A set of experimental batch dissolutions in water of Potassium Sulphate runs were performed to validate the extended model developed. The experiments were performed in the fully baffled, flat-bottomed, cylindrical vessel B, stirred by a Rushton turbine (*D = 0.19* m, *D/T = 0.5*, *c/T = 1/3*). The vessel was provided with a suitable cover to avoid the occurrence of the *surface aeration* phenomenon. Solute concentrations were indirectly detected by means of a conductimetric probe. A data acquisition system was used to record solute concentration dynamics.

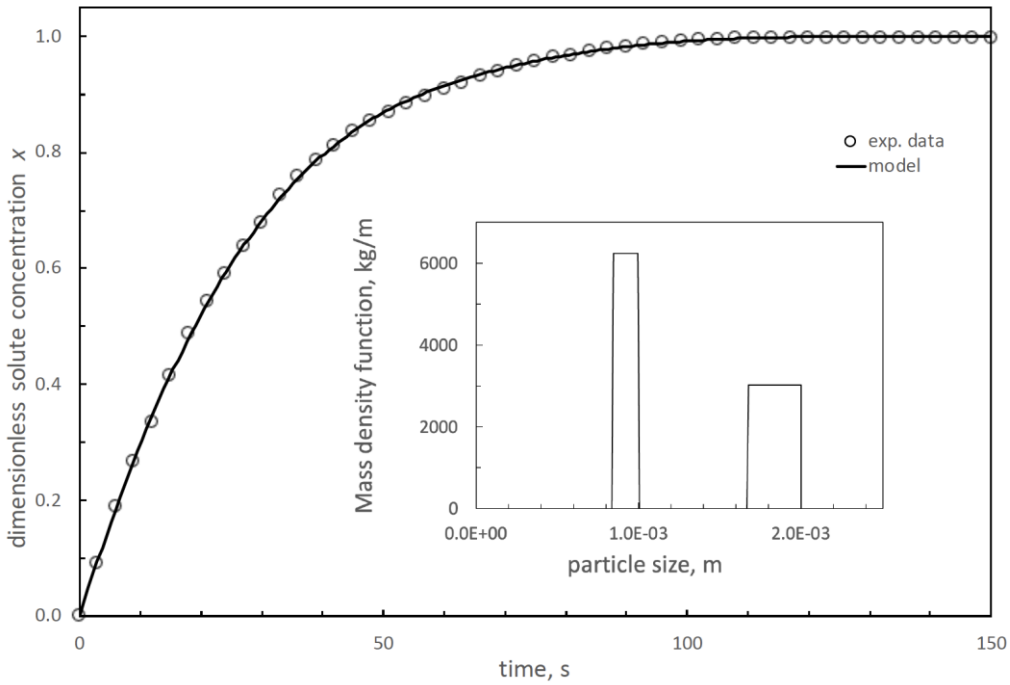

Figure 5: Multi-sized particles dissolution run: comparison between experimental (circles) and model prediction (curve). Potassium Sulphate dissolution in water, d_{p01}=0.925*10^{-3} m (50%w) and d_{p02} = 1.87*10^{-3} m (50%w), C*=0.377 kg/m^3, Vessel B, N=600 rpm.

A typical result is shown in Figure 5, where the experimental dissolution dynamics, at 600 rpm, of a mixture of particles of two different initial sizes is compared with model predictions. As can be seen, a remarkable agreement was obtained between experimental data (empty circles) and model predictions (solid line), after best fitting the value of the mass transfer coefficient, which was consistent with the values obtained for the single-sized particles. All other experimental runs, performed by varying the initial particle size distribution as well as the agitation speed, always resulted in a similar agreement: the extended model could then be considered as being well-validated.

Once the model had been validated, many simulations were run for a given value of the mass transfer coefficient k_c* and for initial distributions of various shapes and widths around a

central “average” size. Each run resulted in a time-concentration curve that was analysed (as a *pseudo-experimental* data set) using the previously described simpler single-sized models, assuming for all particles an initial size equal to the average particle size. In this way *pseudo-experimental* k_c values were obtained, that could be compared with the known exact k_c* value imposed for the predictions. The differences between to two indicated the errors that would have been incurred, in the estimation of the mass transfer coefficient, as a result of the (unaccounted for) spread of the initial particle size distribution. The purpose of these computations was that of establishing the needed narrowness of the initial size distribution to get meaningful results for k_c by the simpler “single-sized” model.

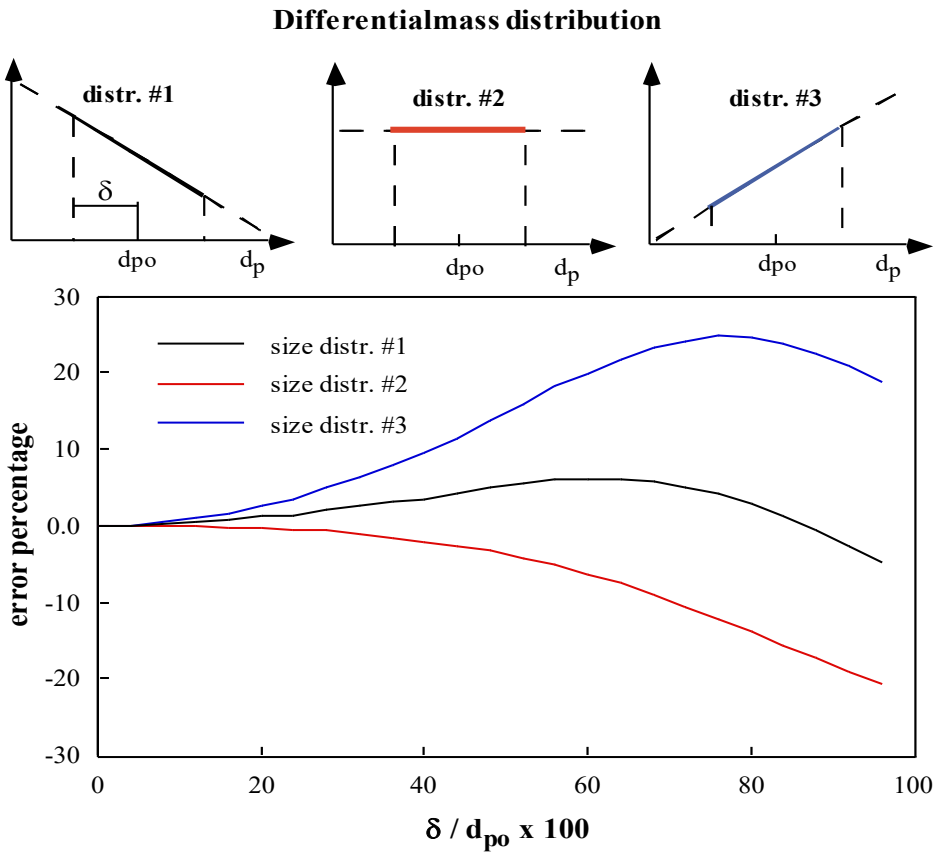

Figure 6: Error incurred in the estimation of solid-liquid mass transfer coefficient when neglecting the initial size distribution of dissolving particles.

Figure 6 presents the results of the computations to determine the error incurred in estimating the mass transfer coefficient (k_c) using the simpler "single-sized" model when there is a spread in the initial particle size distribution. In this case, the arithmetic mean between the two boundary sizes was used as the nominal initial size for all particles. This definition of the average diameter is convenient for sieved particles because it corresponds to the arithmetic mean of the two nominal sieve apertures without requiring information about the distribution shape inside them.

The results demonstrate that the error incurred is relatively small, even for relatively wide initial size ranges. In particular, the error is smaller than 3%, with any of the distributions considered, for a size width of ± 20% around the average diameter. These results retrospectively confirm the validity of the k_c data previously obtained with sieved particles [Brucato *et al.*, 1990; Grisafi *et al.*, 1994; Grisafi *et al.*, 1998] as the size range involved was always narrower than ± 10%.

6. Conclusions

A set of dissolution models has been developed and experimentally validated. All of them were found to be in excellent agreement with experimental findings.

One of these can be employed for simultaneously assessing interfacial concentration and mass transfer coefficient. It was used here to give one of the very few confirmations of the existence of equilibrium conditions at the solid-liquid interface during the dissolution. It was also used to assess the interfacial concentration for a salt for which the equilibrium concentration was not known nor experimentally accessible.

The general applications of this model include:

- Modelling and scale-up of agitated batch dissolution apparatuses;
- Determination of C_i for fundamental research on mass-transfer phenomena (verification of the relevance of interfacial resistances), or for design and development purposes;
- Determination of saturation concentration C_{sat} for systems in which a steady state determination is made difficult due to coupled dissolution and precipitation;

The low final concentration version of the same models has been shown to be particularly useful for k_c assessment when the interfacial concentration is known.

Furthermore, extended models have been developed to simulate dissolution processes involving solid particles of multiple sizes. The main applications of these extended models include:

- Modelling of industrial dissolutions for design purposes;
- Determination of mass transfer coefficient k_c by using un-sieved solid particles for the experimental runs, provided that their size distribution is known;
- Estimation of uncertainty range in data analysis: The extended models help in estimating the uncertainty range when analyzing experimental data obtained with sieved particles, considering the neglected initial particle size distribution.

Overall, these dissolution models offer a versatile and comprehensive framework for studying and understanding dissolution processes, enabling various practical applications and research investigations.

Nomenclature

A = constant in Equation (7) [s^{-1}]

a_v = particle specific area S_p/V_p [m^{-1}]

B = constant in Equation (12) [m/s]

c = .. impeller clearance [m]

C = liquid bulk concentration [kg/m^3]

C^* = liquid phase concentration for total solid dissolution [kg/m^3]

C_i = liquid phase concentration at the interface [kg/m^3]

C_o = liquid phase concentration at time t_o [kg/m^3]

C_{sat} = saturation concentration [kg/m^3]

D = impeller diameter [m]

d_p = particle diameter [m]

d_{p0} = particle diameter at time t_o [m]

$\boldsymbol{J}$ = solute flux at solid-liquid interface [kg m^{-2} s^{-1}]

k_c = liquid phase mass transfer coefficient [m/s]

L = d_p (particle size) in population density equations [m]

M = solid phase mass at time t [kg]

M_0 = solid phase mass at time t=0 [kg]

N = impeller rotational speed [s^{-1}]

n = population density [m^{-4}]

n_o = population density at time zero [m^{-4}]

R = dissolution rate of particles [m/s]

Re_i = impeller Reynolds number $\rho D_i^2 N \mu^{-1}$

S_p = interfacial surface of a particle [m^2]

S_t = total solid interfacial surface [m^2]

t = time [s]

T = vessel diameter [m]

V_p = particle volume [m^3]

V_t = liquid phase volume [m^3]

x = dimensionless concentration

x_i = interfacial dimensionless concentration

Greek letters

α = volume shape factor

β = surface shape factor

δ = half initial size range [m]

ρ_p = particle density [kg/m^3]

References

Baeyens J., Vincent J., Viet A.D.T., Dewil R., (2012), Theory and experiments for dissolving solids in water, Chem.Eng.Comm., **199**, 335-353. https://doi.org/10.1130/MEM74-p1

Barker, J.J. and R.E. Treybal (1960), Mass transfer coefficients for solids suspended in agitated liquids, AIChE J., **6** (2), 289-295. https://doi.org/10.1002/aic.690060223

Brucato, A., Brucato V., Rizzuti L. and Sanfilippo M., (1990), Particle dissolution kinetics inside batch stirred vessels, IChemE Symp. Series , 121, 327-341.

Busciglio A., Grisafi F., Scargiali F., Brucato A., (2010), On the measurement of local gas hold-up and interfacial area in gas–liquid contactors via light sheet and image analysis, Che. Eng. Sci., 65, 3699-3708. https://doi.org/10.1016/j.ces.2010.03.004

Carletti,C., S. Bikić, G. Montante and A. Paglianti (2018), Mass Transfer in Dilute Solid−Liquid Stirred Tanks, Ind. Eng. Chem. Res., 57, 6505−6515. https://doi.org/10.1021/acs.iecr.7b04730

Hormann T., D. Suzzi, and J.G. Khinast (2011), Mixing and Dissolution Processes of Pharmaceutical Bulk Materials in Stirred Tanks: Experimental and Numerical Investigations, Ind. Eng. Chem. Res., 50, 12011–12025. https://doi.org/10.1021/ie2002523

Grisafi, F., A. Brucato, L. Rizzuti (1994), Solid-liquid mass transfer coefficients in mixing tanks: influence of side wall roughness, I. Chem. Symp. Ser., **136**, pp. 571-578.

Grisafi, F., A. Brucato and L. Rizzuti (1998), Solid-Liquid mass transfer coefficients in gas-solid-liquid stirred vessels, Can. J. of Chem. Eng., **76**, 446-455. https://doi.org/10.1002/cjce.5450760315

Hixson, A.W. and J. H. Crowell (1931), Dependence of reaction velocity upon surface and agitation: I- theoretical considerations, Ind. Eng. Chem., **23** (8), 923-931. https://doi.org/10.1021/ie50260a018

Hartmann H., J.J. Derksen, H.E.A. van den Akker (2006), Numerical simulation of a dissolution process in a stirred tank reactor, Chem. Eng. Sci., 61, 3025–3032. https://doi.org/10.1016/j.ces.2005.10.058

Hormann. T, D. Suzzi and J.G. Khinast (2011), Mixing and Dissolution Processes of Pharmaceutical Bulk Materials in Stirred Tanks: Experimental and Numerical Investigations, Ind. Eng. Chem. Res., 50, 12011–12025. https://doi.org/10.1021/ie2002523

Meneses J.P.C.H., Calcada L.A., Scheid C.M., Magalhaes C. (2017), Determination of the convective mass transfer coefficient in the dissolution of NaCl particles in non-Newtonian fluids, J.Nat.G.Sci.&Engng, 45, 118-126. https://doi.org/10.1016/j.jngse.2017.03.014

Montante, G., C. Carletti, F. Maluta, A. Paglianti (2019), Solid Dissolution and Liquid Mixing in Turbulent Stirred Tanks, Chem. Eng. Technol., 42, No. 8, 1627–1634. https://doi.org/10.1002/ceat.201800726

McCabe, W. L., Smith, J. C., and Harriott, P. (2004). Unit Operations of Chemical Engineering, 7th ed., McGraw-Hill, Boston

Nienow A.W. (1975), Agitated vessel particle-liquid mass transfer: A comparison between theories and data. Chem Engng J., 9, 153-160. https://doi.org/10.1016/0300-9467(75)80007-4

Nienow, A.W. and D. Miles (1978), The effect of impeller/tank configurations on fluid-particle mass transfer, Chem. Engng J., **15**, 13-24. https://doi.org/10.1016/0300-9467(78)80033-1

Nikhade B.P. and V.G. Pangarkar (2007), Theorem of corresponding hydrodynamic states for estimation of transport properties: Case study of mass transfer coefficient in stirred tank fitted with helical coil. Ind. Eng. Chem. Res.**,** 46, 3095-3100. https://doi.org/10.1021/ie060385f

Pangarkar, V. G., Yawalkar A. A., Sharma M. M., and Beenackers A. A. C. M., (2002), Particle-Liquid Mass Transfer Coefficient in Two-/Three-Phase Stirred Tank Reactors. Ind. Eng. Chem. Res.**,** *41,* 4141-4167. https://doi.org/10.1021/ie010933j

Paul E.L., Atiemo-Obeng V. A., Kresta S. M., (2003), Handbook of Industrial Mixing: Science and Practice. Wiley Online Library, https://doi.org/10.1002/0471451452

Tamburini A., Cipollina A., Micale G., Brucato A., (2013), Particle distribution in dilute solid liquid unbaffled tanks via a novel laser sheet and image analysis based technique, Chem.Eng.Sci., 87, 341-358. http://dx.doi.org/10.1016/j.ces.2012.11.005

Winterbottom, M., Fishwick, R., Stitt, H., (2003), Solid-liquid mass transfer and hydrodynamics in the hydrogenation of 4-nitrobenzoic acid. Canadian Journal of Chemical Engineering, 81(3-4), 588-596. https://doi.org/10.1002/cjce.5450810334